



Research

Cite this article: Kotani K, Yamaguchi I, Yoshida L, Jimbo Y, Ermentrout GB. 2014 Population dynamics of the modified theta model: macroscopic phase reduction and bifurcation analysis link microscopic neuronal interactions to macroscopic gamma oscillation.

J. R. Soc. Interface **11**: 20140058.

<http://dx.doi.org/10.1098/rsif.2014.0058>

Received: 18 January 2014

Accepted: 27 February 2014

Subject Areas:

biomathematics, biocomplexity

Keywords:

neuronal population, gamma oscillation, macroscopic phase response function, adjoint method, sparse firing

Author for correspondence:

Kiyoshi Kotani

e-mail: kotani@k.u-tokyo.ac.jp

Electronic supplementary material is available at <http://dx.doi.org/10.1098/rsif.2014.0058> or via <http://rsif.royalsocietypublishing.org>.

Population dynamics of the modified theta model: macroscopic phase reduction and bifurcation analysis link microscopic neuronal interactions to macroscopic gamma oscillation

Kiyoshi Kotani^{1,2}, Ikuhiro Yamaguchi¹, Lui Yoshida¹, Yasuhiko Jimbo¹ and G. Bard Ermentrout²

¹Graduate School of Frontier Science, University of Tokyo, Chiba, Japan

²Department of Mathematics, University of Pittsburgh, Pittsburgh, PA, USA

Gamma oscillations of the local field potential are organized by collective dynamics of numerous neurons and have many functional roles in cognition and/or attention. To mathematically and physiologically analyse relationships between individual inhibitory neurons and macroscopic oscillations, we derive a modification of the theta model, which possesses voltage-dependent dynamics with appropriate synaptic interactions. Bifurcation analysis of the corresponding Fokker–Planck equation (FPE) enables us to consider how synaptic interactions organize collective oscillations. We also develop the adjoint method (infinitesimal phase resetting curve) for simultaneous equations consisting of ordinary differential equations representing synaptic dynamics and a partial differential equation for determining the probability distribution of the membrane potential. This method provides a macroscopic phase response function (PRF), which gives insights into how it is modulated by external perturbation or internal changes of parameters. We investigate the effects of synaptic time constants and shunting inhibition on these gamma oscillations. The sensitivity of rising and decaying time constants is analysed in the oscillatory parameter regions; we find that these sensitivities are not largely dependent on rate of synaptic coupling but, rather, on current and noise intensity. Analyses of shunting inhibition reveal that it can affect both promotion and elimination of gamma oscillations. When the macroscopic oscillation is far from the bifurcation, shunting promotes the gamma oscillations and the PRF becomes flatter as the reversal potential of the synapse increases, indicating the insensitivity of gamma oscillations to perturbations. By contrast, when the macroscopic oscillation is near the bifurcation, shunting eliminates gamma oscillations and a stable firing state appears. More interestingly, under appropriate balance of parameters, two branches of bifurcation are found in our analysis of the FPE. In this case, shunting inhibition can effect both promotion and elimination of the gamma oscillation depending only on the reversal potential.

1. Introduction

It is known that various biological systems use collective rhythms that are composed of noisy individual oscillations with their complex interactions [1–4]. Among them, local circuits in the cerebral cortex and hippocampus consist of thousands of interacting excitatory and inhibitory neurons that together often generate macroscopic oscillations called the local field potential (LFP). Many recent experiments have shown that gamma oscillations (30–80 Hz) of the LFP may play functional roles in cognition and/or attention [1,5–7]. Furthermore, inhibitory neurons are known to be a key factor for gamma oscillations [5,8–12], which emerge in the LFP even when individual neurons do not fire

at every gamma cycle [13,14]. This phenomenon is sometimes called sparse firing. Because of the difficulty of mathematical treatments of this type of activity, much remains unknown about the relationship between the physiological properties of synaptic interactions and macroscopic gamma oscillations. The relationship between external inputs (or changes of internal state) and macroscopic response also remains unclear.

In the case of a limit cycle oscillator, the phase response function (PRF), which is also called the infinitesimal phase resetting curve [15], is a powerful tool for investigating how such rhythms are modulated by external interactions [16,17]. With respect to the PRF for population activity, theoretical studies have used the Fokker–Planck equation (FPE) [18–20] to derive macroscopic PRFs and have shed light on the theoretical relationships between the microscopic oscillations and the macroscopic ones. Furthermore, a recent experimental study determined the macroscopic PRF in a local neuronal population in the CA3 region of the hippocampus [21]. Therefore, it is important to develop theoretical frameworks including the derivation of the macroscopic PRFs to achieve an in-depth understanding of the mathematical and physiological relationships between individual neurons or synapses and macroscopic oscillations.

In this study, we focused on a neuron model, the so-called theta model, which has the simplest form as well as equivalent dynamics to the conductance-based Class I neuron models because it is mathematically the normal form of the saddle-node infinite period [15]. We then derived a version of the theta model that incorporates conductance-based synapses, but remains tractable for numerical and mathematical analysis. The advantage of the theta model is that the resulting FPE lies on a circle (periodic boundary conditions) so that there are no discontinuities (as in leaky integrate-and-fire (LIF) models). Furthermore, the continuous nature of the system and its periodicity in phase space allow us to define a related adjoint operator and thus compute macroscopic PRFs. In addition, we can also use numerical continuation to study bifurcations in the model. The model also retains the physiological properties of conductance-based synapses so that properties like shunting inhibition can be analysed.

Next, to obtain macroscopic PRFs for the neuronal population model, the adjoint method was developed for simultaneous equations composed of ordinary differential equations (ODEs) for synaptic dynamics and a partial differential equation (PDE) for determining the probability distribution of the membrane dynamics. After confirming the validity of the proposed analytical frameworks, we focused on the case of an inhibitory population and used the macroscopic PRFs and bifurcation diagrams to investigate how the synaptic rising time constant, synaptic decaying time constant and shunting inhibition affected the macroscopic gamma oscillations. We finally studied locking to periodic stimuli.

2. Material and methods

2.1. Derivation of the modified theta model

We consider a homogeneous network of $N = 1000$ inhibitory neurons as described by the quadratic integrate-and-fire (QIF) model. The QIF model is a representative model of Class I neurons and is widely used for computational studies [22–24]. Here, $V^{(i)}(t)$ denotes the potential of the i th neuron at time t . Then, the

dynamics of $V^{(i)}(t)$ are represented as

$$C \frac{dV^{(i)}(t)}{dt} = g_L \frac{(V^{(i)}(t) - V_R)(V^{(i)}(t) - V_T)}{V_T - V_R} - g_{\text{syn}}^{(i)}(t)(V^{(i)}(t) - V_{\text{syn}}) + I + \sigma \xi^{(i)}, \quad (2.1)$$

where ξ represents stochastic fluctuations with $\langle \xi^{(i)}(t) \rangle = 0$ and $\langle \xi^{(i)}(t) \xi^{(j)}(t') \rangle = \delta_{ij} \delta(t - t')$, σ ($\mu\text{A}\sqrt{\text{ms cm}^{-2}}$) is the magnitude of the fluctuation, $C = 1 \mu\text{F cm}^{-2}$ is the membrane capacitance and I ($\mu\text{A cm}^{-2}$) is a constant current. $g_L = 0.1 \text{ mS cm}^{-2}$ is the leak conductance and g_{syn} is the synaptic conductances. In absence of synapses and external current, the firing threshold is $V_T = -55 \text{ mV}$. That is, when $V(t)$ crosses the threshold, then the voltage grows faster than exponentially and blows up to infinity in a finite amount of time. At this point, $V(t)$ is then reset to $-\infty$ where it will then tend towards V_R . The resting potential V_R is -62 mV . The reversal potential of inhibitory synaptic currents is $V_{\text{syn}} = -70 \text{ mV}$.

The dynamics of the GABAergic (GABA_A) synaptic conductances $g_{\text{syn}}^{(i)}$ are second-order exponentials

$$\tau_r \tau_d \frac{d^2 g_{\text{syn}}^{(i)}(t)}{dt^2} + (\tau_r + \tau_d) \frac{dg_{\text{syn}}^{(i)}(t)}{dt} + g_{\text{syn}}^{(i)}(t) = \bar{g}_{\text{syn}} \sum_k \delta(t - t^{(k)}), \quad (2.2)$$

where $t^{(k)}$ is the firing time of the pre-synaptic cell, $\tau_r = 0.5 \text{ ms}$ is a rise time and $\tau_d = 5 \text{ ms}$ is a decay time [25]. To match the peak conductance of GABA on interneurons to 6.2 nS , which is based on the earlier model and experimental studies [25–27], we set $2.9 \times 10^{-4} \text{ cm}^2$ as the area of a neuron [28] and thus obtained the value $\bar{g}_{\text{syn}} = 0.138 \text{ mS cm}^{-2}$. Under the condition that the synaptic connections between neurons are random with a probability of p_{syn} , it is known that the synaptic influence on each neuron can be homogenized as an approximation [25]. Then, the above equation reads as

$$\tau_r \tau_d \frac{d^2 g_{\text{syn}}(t)}{dt^2} + (\tau_r + \tau_d) \frac{dg_{\text{syn}}(t)}{dt} + g_{\text{syn}}(t) = \bar{g}_{\text{syn}} p_{\text{syn}} \sum_{k=1}^N \delta(t - t^{(k)}). \quad (2.3)$$

Here, we introduce θ that satisfies the relation

$$V^{(i)} = \frac{V_R + V_T}{2} + \frac{V_T - V_R}{2} \tan \frac{\theta^{(i)}}{2}. \quad (2.4)$$

Then, equation (2.1) reads as

$$C \frac{d\theta^{(i)}}{dt} = -g_L \cos \theta^{(i)} + \frac{2}{V_T - V_R} (1 + \cos \theta^{(i)}) (I + \sigma \xi^{(i)}) + g_{\text{syn}} \left[\frac{2V_{\text{syn}} - V_R - V_T}{V_T - V_R} (1 + \cos \theta^{(i)}) - \sin \theta^{(i)} \right]. \quad (2.5)$$

We call this the modified theta model because it is a physiologically precise version of the theta model, which is well known as a reduced model of Class I neurons [15]. It should be noted that the conversion to the modified phase model is valid even under strong noise or synaptic interactions because it is not derived from a phase reduction, which is valid only in the case of weak interactions [11,29,30], but rather by the transformation of variables.

2.1.1. Fokker–Planck equation and macroscopic phase reduction by the adjoint method

We developed an appropriate adjoint method for the population of the neurons, each of which is described by the modified theta model (equations (2.3) and (2.5)). First, we set the current $I = 2$, noise intensity $\sigma = 2$ and probability of connections $p_{\text{syn}} = 0.2$ as nominal values. Physiologically, I , σ and p_{syn} depend on the

state of neurons and networks; therefore, they should be treated more flexibly compared with other parameters. The FPE [31,32] of the neurons and synaptic equation are described as

$$\begin{aligned} \frac{\partial P(\theta, t)}{\partial t} = & -\frac{\partial}{\partial \theta} \left\{ \frac{1}{C} \left[-g_L \cos \theta + c_1(1 + \cos \theta)(I - \frac{c_1 \sigma^2}{2C} \sin \theta) \right. \right. \\ & \left. \left. + g_{\text{syn}}(t)[c_2(1 + \cos \theta) - \sin \theta] \right] P(\theta, t) \right\} \\ & + \frac{c_1^2 \sigma^2}{2C^2} \frac{\partial^2}{\partial \theta^2} [(1 + \cos \theta)^2 P(\theta, t)] \end{aligned} \quad (2.6)$$

and

$$\frac{d^2 g_{\text{syn}}}{dt^2} = c_4 \frac{dg_{\text{syn}}}{dt} + c_3 g_{\text{syn}} + c_5 A(t), \quad (2.7)$$

where $c_1 = 2/(V_T - V_R)$, $c_2 = (2V_{\text{syn}} - V_R - V_T)/(V_T - V_R)$, $c_3 = -1/\tau_r \tau_d$, $c_4 = -(\tau_r + \tau_d)/\tau_r \tau_d$, $c_5 = \bar{g}_{\text{syn}} n_{\text{syn}}/\tau_r \tau_d$, $n_{\text{syn}} = p_{\text{syn}} \times N = 0.2 \times 1000 = 200$ and $A(t)$ is a firing probability of neurons. Because $A(t)$ is obtained by the flux at $\theta = \pi$ [18,33], it satisfies $A(t) = g_L P(\pi, t)/C$.

By introducing $G = (g_1, g_2)^T = (g_{\text{syn}}, dg_{\text{syn}}/dt)^T$, the synaptic dynamics can be re-written as

$$\frac{dG}{dt} = \begin{bmatrix} 0 & 1 \\ c_3 & c_4 \end{bmatrix} G + \begin{bmatrix} 0 \\ (c_5 g_L/C)P(\pi, t) \end{bmatrix}. \quad (2.8)$$

The adjoint method is a useful analytical method for deriving the PRF from a limit cycle oscillator [15]. Recently, it has been extended to the FPE by Kawamura *et al.* [19,20]. In the case of our population model (equations (2.6) and (2.7)), the adjoint equation and the dual product for the adjoint method should be derived as a combination of the conventional adjoint method for ODE [15] and the adjoint method for PDE, which was recently developed [19,20]. First, we introduce $P_0(\theta, t)$ and $G_0(t) = (g_0(t), dg_0(t)/dt)^T$ as the limit cycle solution for P and G . They are defined in the region of $0 \leq t < T_{\text{macro}}$, where T_{macro} is the period of the limit cycle oscillation.

In this article, $t = 0$ is set so that $P_0(\pi, t = 0)$ is the maximum firing probability. P_0 and G_0 satisfy the relations

$$\begin{aligned} \frac{\partial P_0}{\partial t} = & -\frac{\partial}{\partial \theta} \left\{ \frac{1}{C} \left[-g_L \cos \theta + c_1(1 + \cos \theta)(I - \frac{c_1 \sigma^2}{2C} \sin \theta) \right. \right. \\ & \left. \left. + g_0[c_2(1 + \cos \theta) - \sin \theta] \right] P_0 \right\} + \frac{c_1^2 \sigma^2}{2C^2} \frac{\partial^2}{\partial \theta^2} [(1 + \cos \theta)^2 P_0] \end{aligned} \quad (2.9)$$

and

$$\frac{dG_0}{dt} = \begin{bmatrix} 0 & 1 \\ c_3 & c_4 \end{bmatrix} G_0 + \begin{bmatrix} 0 \\ (c_5 g_L/C)P_0(\pi, t) \end{bmatrix}. \quad (2.10)$$

We then decompose $P(\theta, t)$ and G as $P(\theta, t) = P_0(\theta, t) + Q(\theta, t)$ and $G = G_0 + H$ with $H = (h_1, h_2)^T$, respectively. The linearized equations for $Q(\theta, t)$ and H are

$$\begin{aligned} \frac{\partial Q}{\partial t} = & -\frac{\partial}{\partial \theta} \left\{ \frac{1}{C} \left[-g_L \cos \theta + c_1(1 + \cos \theta)(I - \frac{c_1 \sigma^2}{2C} \sin \theta) \right. \right. \\ & \left. \left. + g_0[c_2(1 + \cos \theta) - \sin \theta] \right] Q \right\} \\ & + g_0[c_2(1 + \cos \theta) - \sin \theta] Q \\ & - \frac{\partial}{\partial \theta} \left[\frac{1}{C} [c_2(1 + \cos \theta) - \sin \theta] P_0(t) \right] h_1 \\ & + \frac{c_1^2 \sigma^2}{2C^2} \frac{\partial^2}{\partial \theta^2} [(1 + \cos \theta)^2 Q] \end{aligned} \quad (2.11)$$

$$\text{and} \quad \frac{dH}{dt} = \begin{bmatrix} 0 & 1 \\ c_3 & c_4 \end{bmatrix} H + \begin{bmatrix} 0 \\ (c_5 g_L/C)Q(\pi, t) \end{bmatrix}. \quad (2.12)$$

These equations can be rewritten in matrix representation as

$$\frac{\partial}{\partial t} \begin{bmatrix} Q \\ H \end{bmatrix} = J \begin{bmatrix} Q \\ H \end{bmatrix} = \begin{bmatrix} A_{QQ} & A_{QH} \\ A_{HQ} & A_{HH} \end{bmatrix} \begin{bmatrix} Q \\ H \end{bmatrix}, \quad (2.13)$$

where

$$\begin{aligned} A_{QQ}Q \equiv & -\frac{\partial}{\partial \theta} \left\{ \frac{1}{C} \left[-g_L \cos \theta + c_1(1 + \cos \theta)(I - \frac{c_1 \sigma^2}{2C} \sin \theta) \right. \right. \\ & \left. \left. + g_0[c_2(1 + \cos \theta) - \sin \theta] \right] Q \right\} \\ & + \frac{c_1^2 \sigma^2}{2C^2} \frac{\partial^2}{\partial \theta^2} [(1 + \cos \theta)^2 Q], \end{aligned} \quad (2.14)$$

$$A_{QH}H \equiv \begin{bmatrix} -\frac{\partial}{\partial \theta} \left[\frac{1}{C} [c_2(1 + \cos \theta) - \sin \theta] P_0(t) \right] & 0 \\ 0 & 0 \end{bmatrix} \begin{bmatrix} h_1 \\ h_2 \end{bmatrix}, \quad (2.15)$$

$$A_{HQ}Q \equiv \begin{bmatrix} 0 \\ (c_5 g_L/C)Q(\pi, t) \end{bmatrix} \quad (2.16)$$

$$\text{and} \quad A_{HH}H \equiv \begin{bmatrix} 0 & 1 \\ c_3 & c_4 \end{bmatrix} \begin{bmatrix} h_1 \\ h_2 \end{bmatrix}. \quad (2.17)$$

The phase space of equation (2.13), C_0 , is the direct sum of two subspaces of C_1 and C_2 as

$$C_1 = C([0, 2\pi] \rightarrow \mathbb{R}), \quad (2.18)$$

$$C_2 = \mathbb{R}^2 \quad (2.19)$$

$$\text{and} \quad C_0 = C_1 \oplus C_2 = \left\{ \begin{bmatrix} Q \\ H \end{bmatrix} \mid Q \in C_1, H \in C_2 \right\}. \quad (2.20)$$

Then, their dual spaces are defined as

$$C_1^* = C([0, 2\pi] \rightarrow \mathbb{R}), \quad (2.21)$$

$$C_2^* = \mathbb{R}_2 \quad (2.22)$$

$$\text{and} \quad C_0^* = C_1^* \oplus C_2^* = \{[Q^* \ H^*] \mid Q^* \in C_1^*, H^* \in C_2^*\}. \quad (2.23)$$

It can be analytically confirmed that $[Q \ H]^T = [\partial P_0/\partial t \ dg_0/dt]^T$ is a solution of equation (2.13).

From equation (2.13), the linear operator for this phase space is given as

$$L \begin{bmatrix} Q \\ H \end{bmatrix} \equiv \left[\frac{\partial}{\partial t} - J \right] \begin{bmatrix} Q \\ H \end{bmatrix}. \quad (2.24)$$

By defining the dual product as

$$\left\langle [Q^* \ H^*], \begin{bmatrix} Q \\ H \end{bmatrix}; t \right\rangle = \int_0^{2\pi} Q^*(\theta, t)Q(\theta, t)d\theta + H^* \cdot H, \quad (2.25)$$

the adjoint operator L^* is determined by the relation

$$\left\langle [Q^* \ H^*], L \begin{bmatrix} Q \\ H \end{bmatrix}; t \right\rangle = \left\langle L^* [Q^* \ H^*], \begin{bmatrix} Q \\ H \end{bmatrix}; t \right\rangle \quad (2.26)$$

and the adjoint equation $L^*[Q^* \ H^*] = 0$ is derived as

$$\begin{aligned} \frac{\partial Q^*}{\partial t} = & -\frac{1}{C} \left[-g_L \cos \theta + c_1(1 + \cos \theta)(I - \frac{c_1 \sigma^2}{2C} \sin \theta) \right. \\ & \left. + g_0[c_2(1 + \cos \theta) - \sin \theta] \right] \frac{\partial}{\partial \theta} Q^*(\theta, t) \\ & - \delta(\theta - \pi) \frac{c_5 g_L}{C} h_2^* - \frac{c_1^2 \sigma^2}{2C^2} (1 + \cos \theta)^2 \frac{\partial^2}{\partial \theta^2} Q^*(\theta, t) \end{aligned} \quad (2.27)$$

and

$$\begin{aligned} \frac{dH^*}{dt} = & -H^* \begin{bmatrix} 0 & 1 \\ c_3 & c_4 \end{bmatrix} \\ & + \left[\int_0^{2\pi} \frac{\partial}{\partial \theta} \left[\frac{1}{C} [c_2(1 + \cos \theta) - \sin \theta] P_0(t) \right] Q^* d\theta \ 0 \right]. \end{aligned} \quad (2.28)$$

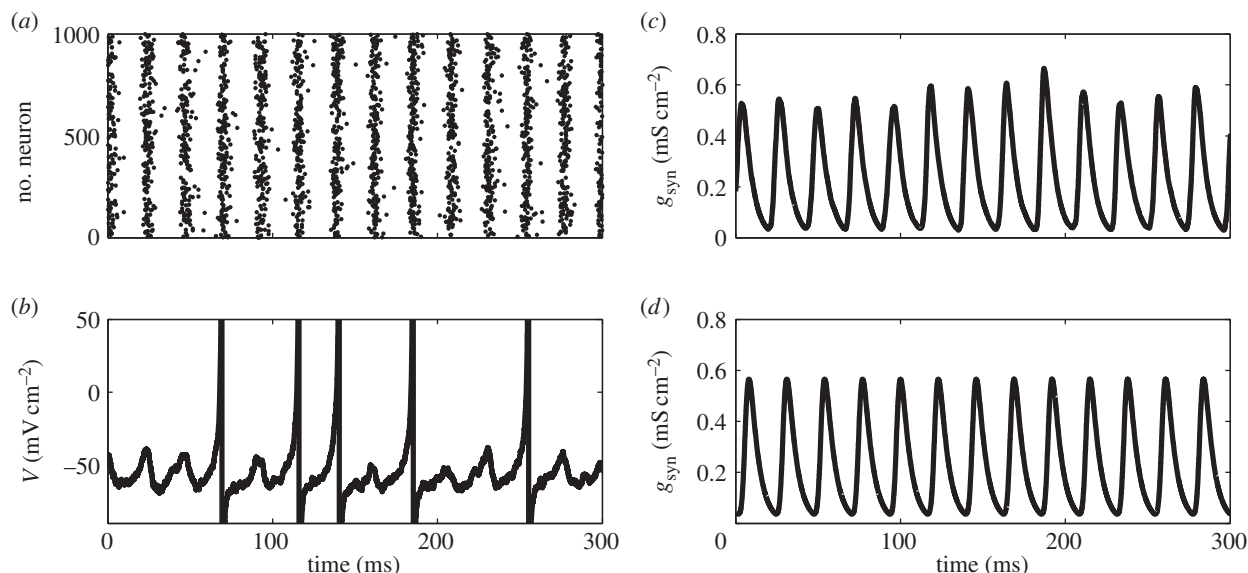


Figure 1. (a) A typical example of the raster plot of the population of modified theta model. (b) Time course of membrane potential of one representative neuron in (a), which is obtained by reversal transform of equation (2.4). Note that individual neurons do not fire in each gamma cycle observed in (a). (c) Time course of the averaged synaptic conductance g_{syn} . (d) Time course of g_{syn} obtained by the corresponding FPE. Note that the time course given by the neuronal model population (c) and by FPE (d) are in a good agreement. All simulations in this figure are executed with nominal values of parameters as $C = 1$, $g_L = 0.1$, $V_T = -55$, $V_R = -62$, $V_{\text{syn}} = -70$, $\tau_r = 0.5$, $\tau_d = 5$, $\bar{g}_{\text{syn}} = 0.138$, $l = 2$, $\sigma = 2$ and $p_{\text{syn}} = 0.2$.

We need the zero eigensolutions of the adjoint equation, $Q_{(0)}^*$ and $H_{(0)}^* = (h_{1(0)}^*, h_{2(0)}^*)$ with the normalizing condition

$$\left\langle [Q_{(0)}^* \ H_{(0)}^*], \left[\frac{\partial P_0}{\partial t} \right]; t \right\rangle = \omega = \frac{2\pi}{T_{\text{macro}}}. \quad (2.29)$$

In actual calculations, we integrate equations (2.27) and (2.28) backwards in time from arbitrary initial conditions to obtain the zero eigensolution (i.e. $Q_{(0)}^*$ and $H_{(0)}^*$) of the adjoint equation, because functional components other than the zero eigensolution have positive eigenvalues; therefore, they eventually vanish (in reverse time).¹

2.1.2. Macroscopic phase response function

Here, we consider the macroscopic PRF. When the external perturbation is added to the equation of synapses, the macroscopic PRF is simply provided by $H_{(0)}^*$. On the other hand, when the external perturbation is applied to all of the neurons, the macroscopic PRF is obtained as

$$Z_{\text{macro}} \left(\theta = \frac{2\pi t}{T_{\text{macro}}} \right) = \int_0^{2\pi} u(\theta) P_0(\theta, \Theta) \frac{\partial}{\partial \theta} Q_{(0)}^*(\theta, \Theta) d\theta, \quad (2.30)$$

where $u(\theta) = c_1(1 + \cos\theta)/C$ is the sensitivity of a single neuron to the phase θ [20]. This equation provides unique insights into how the external perturbations and/or changes of internal states affect macroscopic properties of gamma oscillations and will be discussed in following sections.

3. Results

In order to study the dynamics of large networks of neurons with synaptic coupling, we have extended the so-called theta model (a continuous version of the QIF) to incorporate conductance-based synapses. We did this in order to explore how aspects of synaptic coupling, for example shunting inhibition, affect the ability of inhibitory networks to produce population rhythms. The advantages of the theta model over other simple spiking models are that the model is continuous and certain numerical computations are much

easier. For large numbers of neurons with random coupling, we can reduce the system to a single PDE for the firing rate and synaptic activity (see Material and methods). We can thus turn the focus onto the dynamics of a deterministic system for which there are many available tools.

3.1. Population dynamics of the modified theta models

The numerical computation results for the population of the modified theta models (equations (2.3) and (2.5)) with nominal values of parameters are shown in figure 1a,c, where the macroscopic gamma oscillation can be observed. In figure 1c, we plot the total synaptic conductance as a macroscopic version of the population dynamics. Figure 1b shows an example of the membrane potential of a single neuron, which is obtained by reversal transform of equation (2.4). We can see that in this parameter set, there is sparse firing in which the individual neurons do not fire at every gamma cycle. We also confirmed that the numerical simulation of the corresponding FPE (equations (2.6) and (2.7)) accurately matches the simulated population dynamics (figure 1d). Because our model does not incorporate the effect of resetting and a refractory period, an equivalent representation of this model with resetting and a refractory period is discussed in the electronic supplementary material, text S1 and figure S1.

3.2. Bifurcation diagrams of gamma oscillation

As we are looking only at an inhibitory network (with no 'exotic' currents like the calcium T-current), the network needs tonic drive and feedback inhibition in order to produce population rhythms. Thus, with no synaptic coupling or with reduced drive, the network will produce asynchronous constant in time dynamics. However, as the drive increases and with sufficient negative feedback, a population rhythm emerges through a loss of stability of the constant asynchronous state via a Hopf bifurcation (HB). Thus, we wish to study the stability of the constant asynchronous state as the

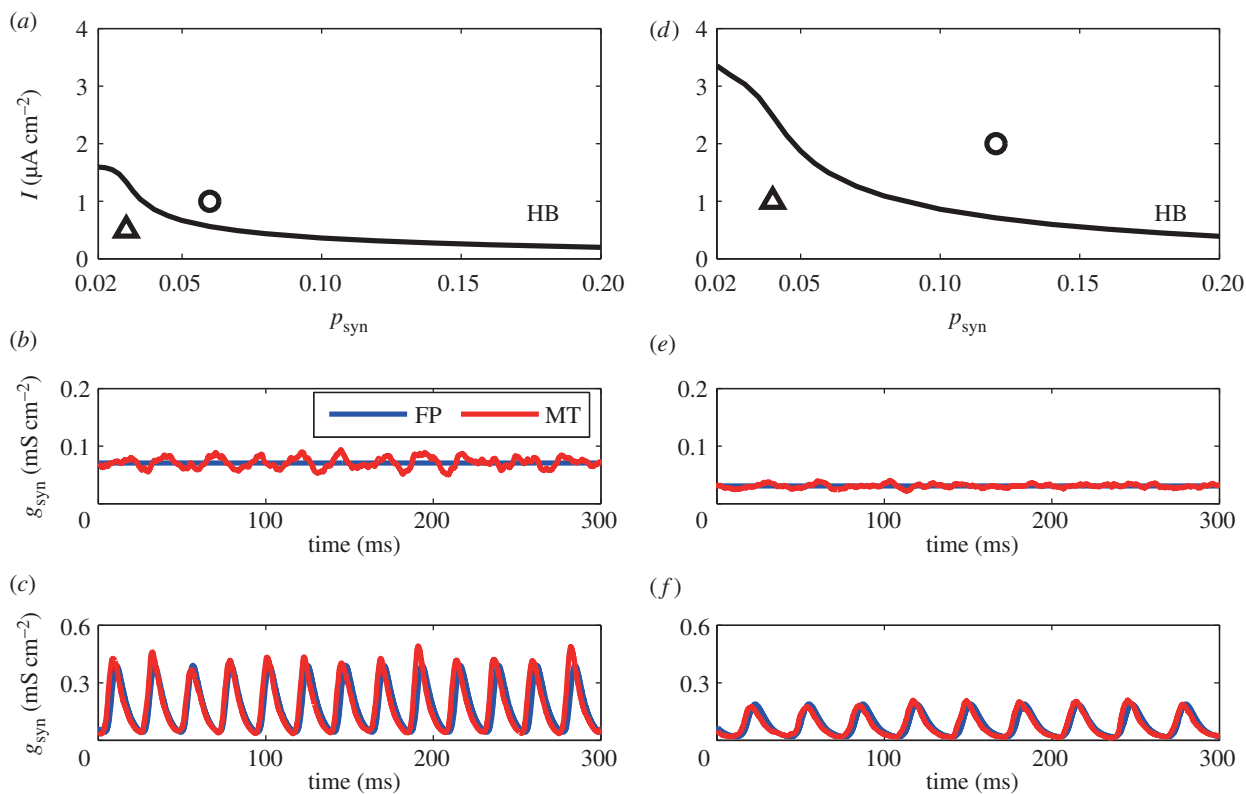


Figure 2. (a) Bifurcation diagram with $\sigma = 1$. HB, Hopf bifurcation. (b,c) Time course of the averaged conductance g_{syn} in the stable region (b) and unstable region (c) by the Fokker–Planck (FP) equation and the modified theta (MT) model. $(p_{\text{syn}}, I) = (0.03, 0.5)$, plotted as a triangle in (a), are adopted for (b) and $(p_{\text{syn}}, I) = (0.06, 1.0)$, circle in (a), are adopted for (c). (d) Bifurcation diagram with $\sigma = 2$. HB, Hopf bifurcation. (e,f) Time course of the averaged conductance g_{syn} in the stable region (e) and unstable region (f) by the FP equation and the MT model. $(p_{\text{syn}}, I) = (0.04, 1.0)$, plotted as a triangle in (d), are adopted for (e) and $(p_{\text{syn}}, I) = (0.12, 2.0)$, circle in (d), are adopted for (f). Besides σ , p_{syn} and I , parameters in this figure are set as nominal values (i.e. the same as figure 1). (Online version in colour.)

drive and negative feedback change. The parameter regions for macroscopic gamma oscillations can be identified by bifurcation analyses of the discretized FPEs [31,34].¹ We chose the applied current, I , and the connection probability, p_{syn} , as two parameters of interest. We note that p_{syn} essentially sets the magnitude of the synaptic connections via the quantity c_5 in the FPE (equations (2.6) and (2.7)). By varying, say, I with p_{syn} fixed, we detect HBs. We then compute a two-parameter curve of HBs as a function of the two parameters I and p_{syn} . Figure 2a,d shows the two-parameter curve for noise amplitudes, $\sigma = 1, 2$. Below the curve (small inputs and sparse connectivity), the constant asynchronous state is stable and above it, there will be oscillations in g_{syn} and thus any macroscopic measure of the behaviour. We also see that the numerical computations of the modified theta models (equations (2.3) and (2.5)) follow the bifurcation analyses and the numerical solutions of the FPE. The small fluctuations in both the stable regions (figure 2b,e) and the gamma oscillatory region (figure 2c,f) are due to the finite-size effect. We note that the curve of HBs is raised up in the higher noise case which means that larger inputs and more densely connected networks are needed for gamma oscillations to emerge and overcome the stability of the asynchronous state.

3.3. Macroscopic phase response function by the adjoint method

The adjoint method provides a rigorous technique for the determination of the PRF and has been successfully applied to individual neural oscillators. The PRF of an oscillating system

measures the shift in timing of the oscillation owing to a stimulus delivered at a specified phase in the ongoing oscillation. The solution to the adjoint equation is proportional to the PRF when the perturbations are small and, thus, the PRF is useful in determining, for example, how changes in the parameters affect the frequency of an oscillator or whether or not it will lock onto a periodic stimulus. For the coupled PDE/ODE system in our population model, obtaining the adjoint solution requires solving a certain linear PDE along with some normalization requirements. We solve the linear PDE by backwards integration (see Material and methods) and to check whether we have found the correct solution, we need to look at an inner product that involves both the solution to the adjoint and the population oscillation. We confirmed the validity of the adjoint method developed in this study by the dual product of the zero eigenfunction and its dual and comparison with the phase shift occurring when a perturbation is applied. Figure 3a shows a two-dimensional solution $Q_{(0)}^*$ of the adjoint method, and figure 3b shows one-dimensional solutions of $H_{(0)}^*$. To check the numerical computation, we checked to see whether equations (2.25) and (2.29) were satisfied for each state on the limit cycle orbit. Figure 3c shows that the sum of the two terms corresponding to $Q_{(0)}^*$ and $H_{(0)}^*$ is, indeed, constant for all time.

Equation (2.30) provides a formula for the PRF of the network when an identical current perturbation is applied to every cell. Thus, we can compare this bulk PRF to the phase shifts induced by a direct perturbation of the network with a short current injection. Therefore, another confirmation of the adjoint method was performed by comparison with PRFs by direct perturbation of the FPE (equations (2.6) and (2.7)) and the results are shown in

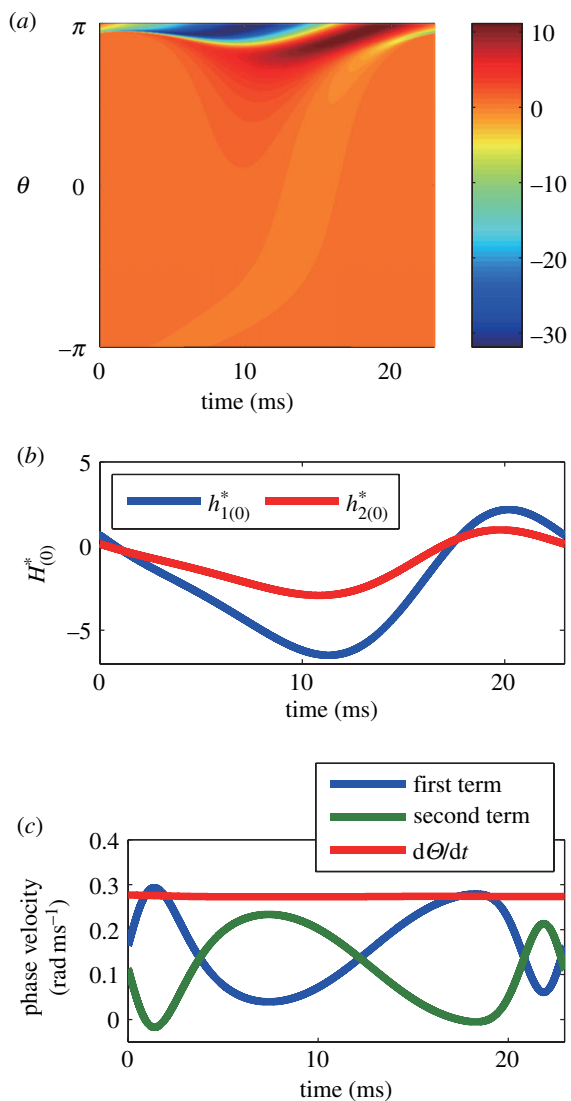


Figure 3. (a,b) A zero eigensolution of the adjoint equation. (a) is $Q_{(0)}^*(\theta, t)$ and (b) is $H_{(0)}^*$. (c) Dual product of zero eigensolution and its dual. The red line is the total sum of the dual product defined in equation (2.25), while the blue line is the first term and the green one is the second term. The flatness of the red line suggests that the macroscopic phase advances constantly in time and consequently indicates the appropriateness of the adjoint method. Parameters in this figure are set as nominal values.

figure 4a. We applied a square wave (amplitude 50, duration 0.01 ms) current pulse to the whole population at different points in the cycle and used this to compute the phase shift and the approximate PRF. Both PRFs determined by the adjoint method (with discretization of the PDE into 200 and 5000 bins) coincided with the results obtained by the direct perturbation of the FPE, which again indicated the appropriateness of the adjoint method. Similarly, the validity of $h_{2(0)}^*$ was confirmed by the perturbation (amplitude 2, duration 0.01 ms) to the left hand side of equation (2.7) (figure 4b).

One of the main purposes for computing the PRF is to study the effects of coupling and periodic forcing of oscillatory systems. Coupling between inhibitory networks could be studied using this method, but, as most coupling between populations is mediated by excitatory outputs, we will not pursue the coupled problem further. However, periodic driving can also be analysed using the method and the experimental driving of inhibitory populations is possible [12]. Thus, to further test the utility of the adjoint method as a means of studying populations, we applied a weak

sinusoidal current to the full population. We used current $I(t)$ in equation (2.6) as

$$I(t) = I_0 + I_{\text{app}} \sin(\omega_{\text{app}} t), \quad (3.1)$$

where $I_0 = 2$ and I_{app} and ω_{app} are the amplitude and frequency of the sinusoidal oscillation, respectively. The region of synchronization can be analytically estimated by the phase coupling function obtained by convolving the periodic current with the PRF [16,17]. The coupling function is defined as

$$\Gamma(\Phi) = \frac{1}{2\pi} \int_0^{2\pi} Z_{\text{macro}}(\Theta) \sin(\Theta + \Phi) d\Theta, \quad (3.2)$$

where $Z_{\text{macro}}(\Theta)$ is the macroscopic PRF equation (2.30). $\Gamma(\Phi)$ is shown in figure 4c. The maximum and the minimum value of Γ indicate tolerance of frequency mismatches between ω_{app} and the natural frequency of gamma oscillation without oscillatory inputs, ω_{nat} , for synchronization to a unit amplitude of oscillation (i.e. $I_{\text{app}} = 1$). That is, if the frequency difference is greater or less than the magnitude of Γ , then 1:1 locking is not possible.

Figure 4d shows the result of both the theory based on equation (3.2) and direct simulation of the FPE. We plot the difference between the network frequency and the forcing frequency as a function of the difference between the natural (with $I_{\text{app}} = 0$) and the forcing frequency. We can see that the synchronized region by numerical computations matches the analytical prediction, which is inside of the black thick lines.

3.4. Modulation of gamma oscillation by varying synaptic time constants

We used the macroscopic PRF obtained by adjoint method to predict the effect of changing the synaptic time constant on the frequency of gamma oscillation.

We denote $R_r(t)$ as the sensitivity of the small change in τ_r to d^2g/dt^2 . This sensitivity can be derived as the partial differentiation of d^2g_0/dt^2 by τ_r and turns out to be

$$R_r(t) = \frac{1}{\tau_r^2} \frac{dg_0}{dt} + \frac{1}{\tau_r^2 \tau_d} g_0 - \frac{\bar{g}_{\text{syn}} n_{\text{syn}} g_L}{\tau_r^2 \tau_d C} P_0(\pi, t). \quad (3.3)$$

Therefore, the frequency changes of the macroscopic oscillation are evaluated as

$$\frac{\partial \omega}{\partial \tau_r} = \frac{1}{T_{\text{macro}}} \int_0^{T_{\text{macro}}} h_{2(0)}^* R_r(t) dt. \quad (3.4)$$

Similarly, the influence of τ_d on the period of the macroscopic oscillations can be obtained by

$$\frac{\partial \omega}{\partial \tau_d} = \frac{1}{T_{\text{macro}}} \int_0^{T_{\text{macro}}} h_{2(0)}^* R_d(t) dt, \quad (3.5)$$

with

$$R_d(t) = \frac{1}{\tau_d} \frac{dg_0}{dt} + \frac{1}{\tau_r \tau_d^2} g_0 - \frac{\bar{g}_{\text{syn}} n_{\text{syn}} g_L}{\tau_r \tau_d^2 C} P_0(\pi, t). \quad (3.6)$$

Figure 5 shows the frequency of the macroscopic oscillation with different values of τ_r and τ_d obtained by numerical computation of the population of the modified theta model as well as those analytically predicted by the phase reduction. The slopes of the straight lines were obtained by equations (3.4) and (3.5) with the nominal values of parameters ($\tau_r = 0.5$ and $\tau_d = 5$). In both cases in which τ_r and τ_d were changed, the numerical computations

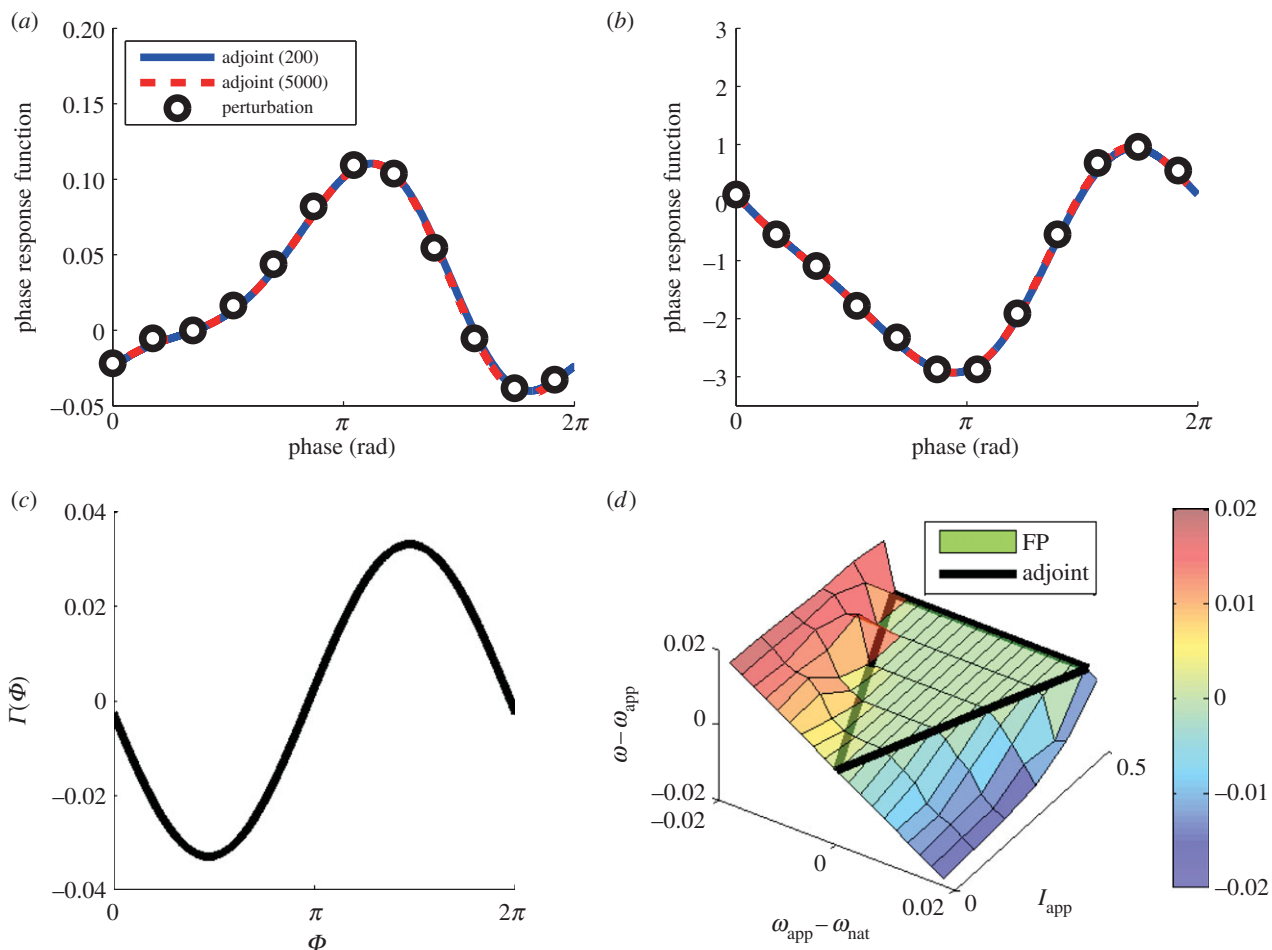


Figure 4. (a,b) Macroscopic PRFs by perturbations to I in (a) and the synaptic function (i.e. the left hand side of equation (2.7)) in (b). The black open circles are the results of direct perturbations of the FPE (equations (2.6) and (2.7)). The blue solid line shows the macroscopic PRF by the adjoint method with 5000 bins for dividing the phase $(-\pi, \pi]$, while the red dotted line shows that with 200 bins. In (a,b), the adjoint method matches the result of the direct perturbation of the FPE. The agreement of the adjoint method with 200 and 5000 bins indicates that 200 bins is enough to calculate macroscopic PRFs. (c) The phase coupling function against oscillatory sinusoidal inputs. (d) The frequency differences between applied oscillation and numerically obtained gamma oscillation by equations (2.6), (2.7) and (3.1) with different inputs of amplitude and frequency. The region that is inside of the black thick lines is the analytically derived synchronized region by the phase reduction theory. There is no frequency difference inside of the black triangle, indicating synchronization is confirmed by the numerical computation of the FPE. Parameters in this figure are set as nominal values without oscillatory current I in (d).

matched the analytical predictions provided by the phase reduction across almost the entire region. The discrepancy at $\tau_r = 0.1$ could be due to the fact that τ_r is getting close to zero where the model is singular. The plots nevertheless show that the population PRF can be used to estimate the frequency dependence on the characteristics of the synaptic inhibition.

To capture the influence of changing τ_r and τ_d on the macroscopic frequency in a wide parameter range of gamma oscillation, we evaluated $\Delta\omega_r$ and $\Delta\omega_d$ as

$$\Delta\omega_r = \left. \frac{\partial\omega}{\partial\tau_r} \right|_{t_r=0.5, t_d=5.0} \quad \text{and} \quad \Delta\omega_d = \left. \frac{\partial\omega}{\partial\tau_d} \right|_{t_r=0.5, t_d=5.0} \quad (3.7)$$

by the adjoint method when changing I and p_{syn} with different values of σ (figure 6a,b,d,e). We confirmed that the signs of $\Delta\omega_r$ and $\Delta\omega_d$ were always negative over the entire regions shown in figure 6. In addition, $\Delta\omega_r/\Delta\omega_d$ (figure 6c,f) varies between 0.85 and 1.87. It was larger than 1 over the almost the entire regions. However, it was smaller than 1 with $I \simeq 1$ and $\sigma = 1$. In general, $\Delta\omega_r/\Delta\omega_d$ increased with increasing I and σ , whereas it was less affected by p_{syn} .

3.5. Effect of shunting inhibition

Experimental evidence has shown that the GABA synapses sometimes increase membrane potential for $V_R \leq V_{syn}$ [35]. This phenomenon is called shunting inhibition, and it was recently argued that it promotes macroscopic gamma oscillation by improving its robustness [35]. Here, we test this hypothesis using the FPE.

First, we numerically solved the FPE and evaluated the maximum firing probability, the average firing probability and ω as in figure 7a,b in the range of $-70 \leq V_{syn} \leq -55$. Increasing the maximum value of the firing probability indicates that the amplitude of the gamma oscillation increases, which means that the robustness of the gamma oscillation is increased by shunting inhibition. The average firing probability and ω also increase as V_{syn} increases. These properties of shunting inhibition are the same as those reported previously [35].

Next, we evaluated the PRFs with shunting inhibition as shown in figure 7c. As V_{syn} increases, the amplitudes of PRF become smaller while maintaining the waveform, indicating that the phase of the oscillation is stable and robust against external interactions. (The larger is the PRF, the more sensitive is the oscillator.) Therefore, the results of PRF also

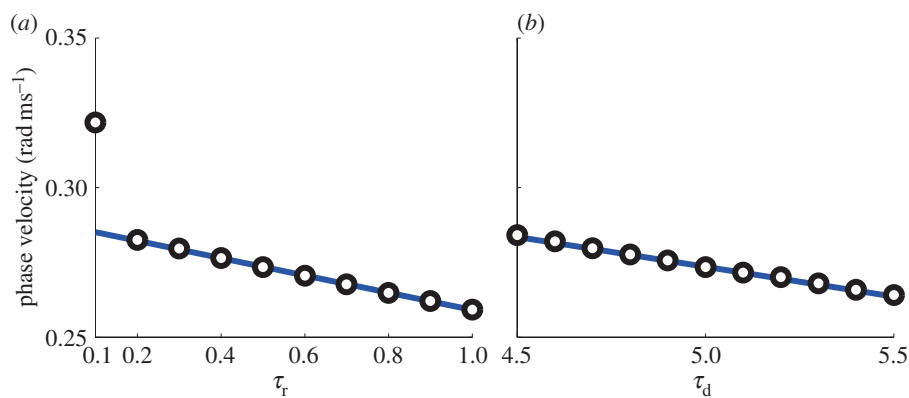


Figure 5. Period of the macroscopic oscillations by changing τ_r (a) and τ_d (b). The circles are obtained by the direct numerical computations of the population of the modified theta model, while the solid lines are analytical predictions by the adjoint method. (Online version in colour.)

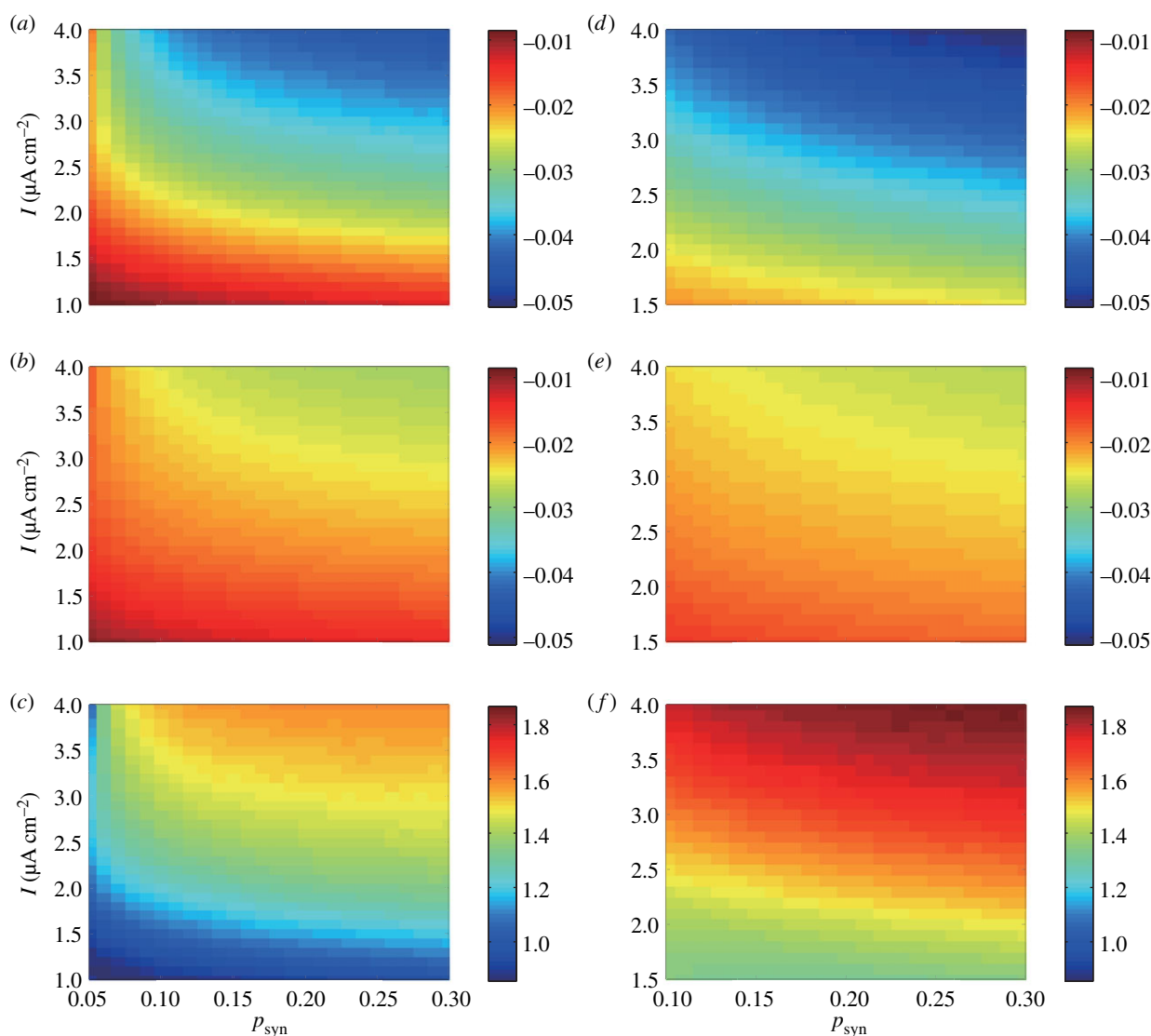


Figure 6. (a,b) $\Delta\omega_r$ in (a) and $\Delta\omega_d$ in (b) with $\sigma = 1$. (d,e) $\Delta\omega_r$ in (d) and $\Delta\omega_d$ in (e) with $\sigma = 2$. (c,f) Ratio of the influence of changing synaptic time constant to gamma oscillation frequency ($\Delta\omega_r/\Delta\omega_d$). $\sigma = 1$ in (c) and $\sigma = 2$ in (f). The parameter regions are determined by referring to the bifurcation diagrams for macroscopic oscillatory region in figure 2a,d; therefore, $1 \leq I \leq 4$ and $0.05 \leq p_{syn} \leq 0.3$ are adopted for (a–c), while $1.5 \leq I \leq 4$ and $0.1 \leq p_{syn} \leq 0.3$ are for (d–f). Besides τ_r , τ_d , σ , p_{syn} and I , parameters in this figure are set as nominal values.

support the finding that shunting inhibition improves the robustness of the gamma oscillations. The maximum value of PRF almost remains constant in the first part of the shunting inhibition in the range of $V_{syn} < -62.5$ mV and decreases in the range of $V_{syn} > -62.5$ mV (figure 7d), which differs from the other indexes (maximum, average of firing

probability and ω) that are monotonic over the entire range of $-70 \leq V_{syn} \leq -55$.

We computed the bifurcation diagram for the FPE using V_{syn} as a parameter and changing the other parameters to investigate whether the above effects of shunting inhibition hold in general. Surprisingly, when we set $p_{syn} = 0.05$, $I = 2$,

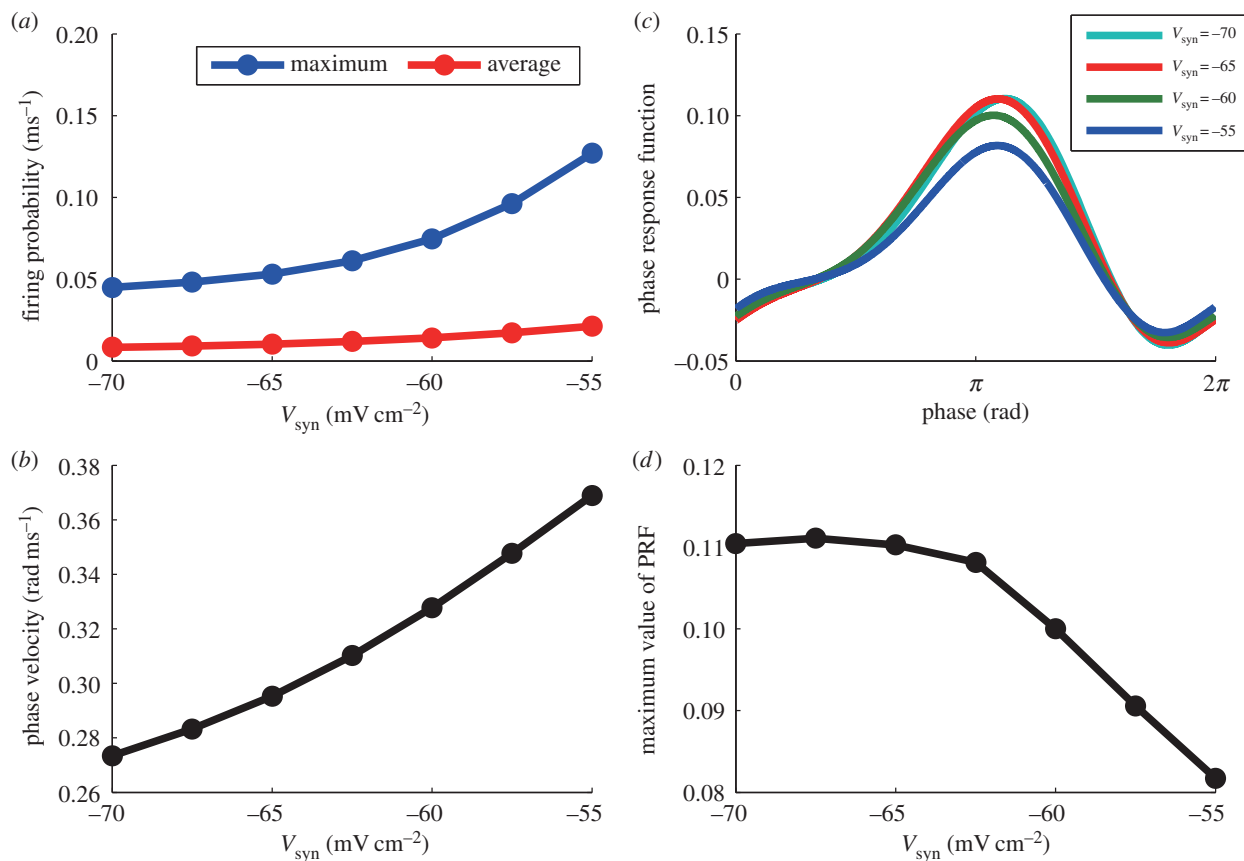


Figure 7. (a) Average and maximum firing probability with different values of V_{syn} . (b) ω with different values of V_{syn} . (c) PRFs against perturbations to I provided by the adjoint method with different values of V_{syn} . (d) Maximum value of PRF with different values of V_{syn} . Besides V_{syn} parameters in this figure are set as nominal values.

the gamma oscillation disappeared above $V_{\text{syn}} \simeq -69.0$ mV and a stable fixed firing state appeared (figure 8a–d). This result means that increasing V_{syn} can destroy the macroscopic gamma oscillation, which is in contrast to the study by Vida *et al.* [35]. More interestingly, when we increased the current to $I=3$ with the same synaptic probability, there were two branches of HB for the macroscopic oscillations: below $V_{\text{syn}} \simeq -63.0$ mV and above $V_{\text{syn}} \simeq -56.5$ mV. Between these bifurcations, there was a region that had a stable fixed firing state (figure 8e–h), although the numerical computation fluctuated near the gamma frequency because of the vicinity of the bifurcation point and the finite-size effect. Therefore, the effect of shunting inhibitions is largely altered by the balance of the inhibitory synapses p_{syn} and current I . Finally, the stable region and oscillatory region are shown in the two-dimensional bifurcation diagram for I and V_{syn} (figure 8i).

4. Discussion

In this study, we first derived a modified theta model that possesses voltage-dependent dynamics and appropriate forms and strengths of the synaptic interactions. These properties are not incorporated into the conventional theta model which is the normal form for the saddle-node infinite cycle bifurcation [15]. Unlike related integrate-and-fire models with conductance-based synapses, the modified theta model is continuous with no resetting. By letting the number of neurons tend to infinity, we derived a hybrid PDE/ODE for the coupled neurons and their synaptic gates. The PDE for the population dynamics has simple

periodic boundary conditions, and because it is continuous, requires no special methods for solving it. Furthermore, solutions to the discretized PDE can be numerically continued and bifurcations are easily detected using AUTO or other packages. Thus, we were able to find the parameter regions for macroscopic gamma oscillations and show that these arise via a supercritical HB. We found that the macroscopic oscillation tends to emerge with larger currents (I), higher rates of synaptic couplings (p_{syn}) and the weaker noise (σ). These results match the experimental findings that the pharmacological activations of interneurons by agonist of metabotropic glutamate receptors or kainate receptors induce large amplitude gamma oscillations and the loss of their interactions by GABA_A receptor antagonist bicuculline eliminates such inhibition-based gamma oscillations [8–10]. Thus, the analyses of the proposed model aid our understanding of the mechanism by which the inhibition-based gamma oscillation arises.

Populations of neurons are subject to external perturbations, so it is important to understand how perturbations affect the population rhythm. For limit cycle oscillations, the PRF describes how perturbations shift the timing of the rhythm. In the limit of short, weak perturbations, the shift in timing is described by the solution to the adjoint equation for the linearization about the limit cycle. Here, we derived the adjoint equation for the linearized Fokker–Planck and synaptic equations along with the limit cycle orbit. Accurate PRFs for the macroscopic oscillation are provided by solutions to the adjoint equation. As the adjoint method for solving a combined problem of ODE and PDE has not been described, we successfully developed a method by

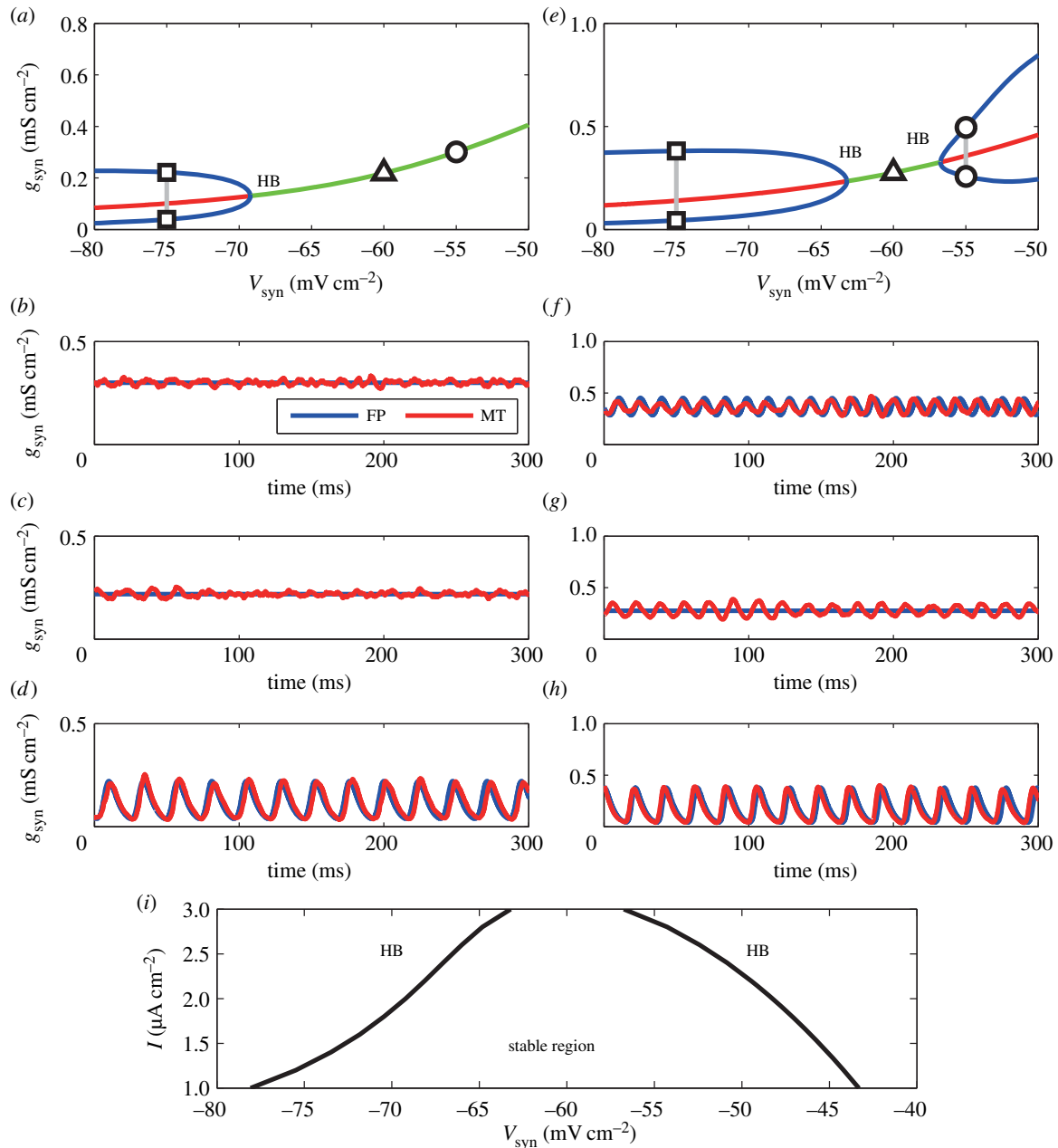


Figure 8. Bifurcation diagrams with $(p_{synr}, I) = (0.05, 2)$ in (a) and with $(p_{synr}, I) = (0.05, 3)$ in (e). (a,e) The green line is a stable fixed solution and the red one is an unstable one. The blue lines indicate the upper bound and lower bound of the Hopf oscillation. HB, Hopf bifurcation. (b–d) Time course of the conductance g_{syn} obtained by the Fokker–Planck (FP) equation and the modified theta (MT) model. $V_{syn} = -55$ mV in (b,f), $V_{syn} = -60$ mV in (c,g) and $V_{syn} = -75$ mV in (d,h). In the case of $(p_{synr}, I) = (0.05, 2)$ (in (a)), as V_{syn} is increased, the gamma oscillation disappears above $V_{syn} \simeq -69.0$ mV and a stable fixed firing mode emerges. On the other hand, when we adopt $(p_{synr}, I) = (0.05, 3)$ (in (e)), gamma oscillations appear in both regions below $V_{syn} \simeq -63.0$ mV and above $V_{syn} \simeq -56.5$ mV. Between them, a stable fixed firing state appears in the solution of the FPE. (i) Two-dimensional bifurcation diagram for shunting inhibition. In the region of $1 \leq I \leq 3$ and $-80 \leq V_{syn} \leq -40$, there are two Hopf oscillatory regions and there is a stable state between them. Besides V_{synr} , p_{synr} and I , parameters in this figure are set as nominal values.

introducing the appropriate dual product. The validity of the derived PRFs was confirmed by the dual product of zero eigensolution and its dual (figure 3c), by direct perturbation of the FPE (figure 4a,b), by the region of synchronization to oscillatory inputs (figure 4d) and by the frequency shift caused by changing the synaptic time constants (τ_r and τ_d) to the population of the modified theta model (figure 5a,b). Although the PRF derived by the adjoint method is generally used to evaluate the effect of external perturbations [16,17], in our study, the macroscopic PRF was successfully applied to evaluate not only the effects of external perturbations but also how intrinsic parameter changes alter the

macroscopic oscillatory dynamics. Recent experiments have used optogenetic tools to selectively drive subpopulations of neurons with periodic stimuli [12,21,36]; the adjoint method allows us to investigate the effects of such perturbations on the macroscopic gamma oscillations analytically.

Many studies have used the LIF model [25,35,37] or other neuronal models [26,38] to investigate the properties of population rhythms. Their analyses have often been confined to simulations of the population of individual neurons. This is partly because the FPEs for their models require complex boundary conditions, which makes mathematical and numerical treatments somewhat limited. In particular, it is

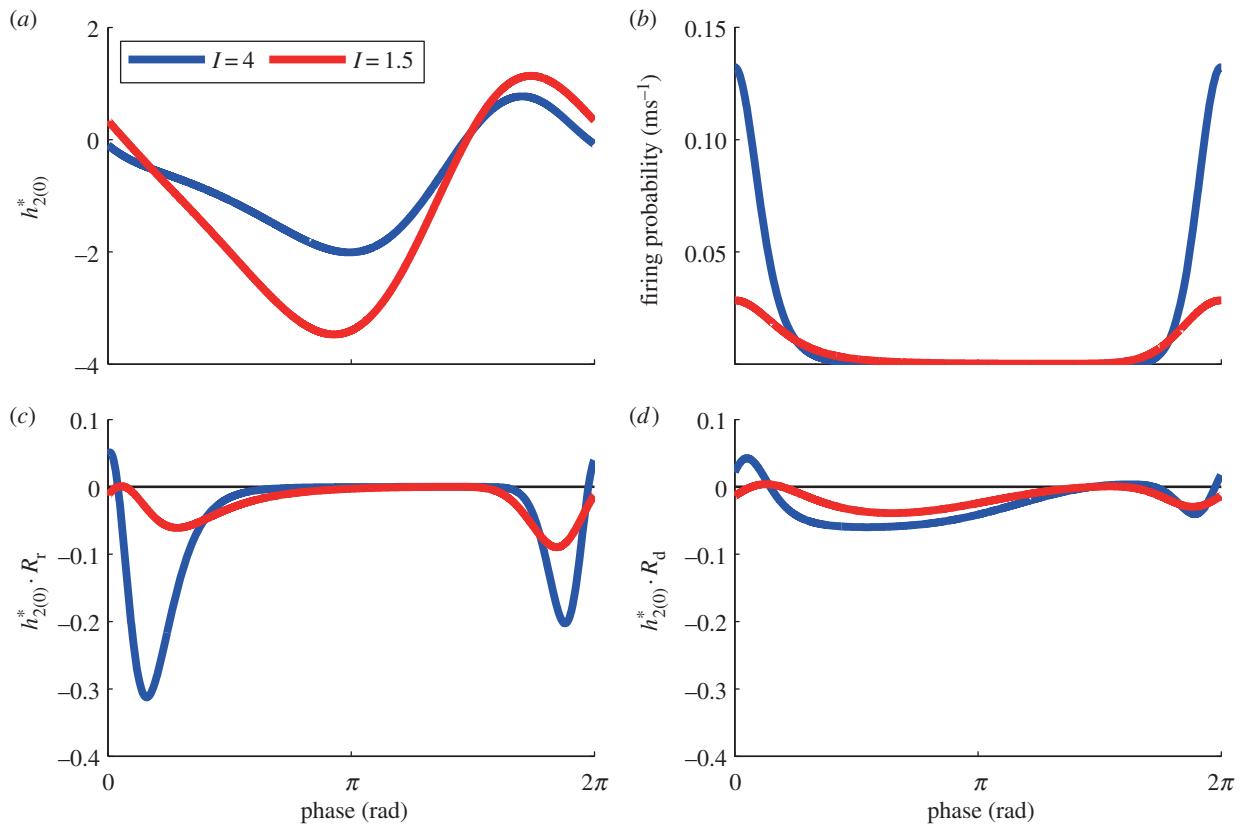


Figure 9. (a) PRFs ($h_{2(0)}^*$). (b) Firing probability $g_L P(\pi, t)/C$ of the periodic orbit. (c) Time course of $h_{2(0)}^* \cdot R_r$. (d) Time course of $h_{2(0)}^* \cdot R_d$. In all panels, the blue line is provided by $I = 4$, while the red one is provided by $I = 1.5$. The horizontal axis in all panels is normalized from 0 to 2π . In (c), we can see that there are large negative peaks with $I = 4$, which would be because of sharp peaks for firing probability and synaptic influences. Besides I , parameters in this figure are set as nominal values.

hard to perform numerical bifurcation analysis on these PDEs. Although Brunel *et al.* derived the spike rate response from the FPE to evaluate the properties of the population of the LIF model [25,37], the resulting formulae are complicated and also valid only in the linear regime. By contrast, the population activity of the standard theta model is rather easily numerically analysed because the corresponding FPE can be treated with periodic boundary conditions and has no discontinuities [18,31,39]. The physiological origin of the gamma oscillations is not easy to discuss in the conventional theta model because the synaptic activity comes through additive currents rather than conductance-based synapses. By contrast, the modified theta model and its analytical framework developed in this study provide mathematically rigorous analyses for determining how collective dynamics depend on physiologically relevant parameters. Some theoretical work has been done on this with regard to inhibitory networks. Brunel *et al.* [25] showed that increases of the rise (τ_r) and decay (τ_d) times of GABA synapses decreased the frequency of gamma oscillations and that the sensitivity of τ_d was much lower than that of τ_r . Maex *et al.* also demonstrated a significant frequency decrease by increasing τ_d [40]. Using the adjoint method, we derived expressions for the sensitivity of the frequency to the synaptic time constants (figure 6). Our results, like those of previous authors, show that the frequency decreases with the increase in both the synaptic decay and the synaptic rise time. We also showed that the ratio of the sensitivities to the time constants, $\Delta\omega_r/\Delta\omega_d$, is smaller than 1; i.e. the changes in τ_d affect the oscillatory frequency more than τ_r , under the condition of weak current

($I \simeq 1$) and noise ($\sigma = 1$). This result differs from that of Brunel *et al.* [25], who focused on much higher frequency (more than 100 Hz) states of gamma oscillation where the slower scale of the decay time may not be as relevant.

In a pair of comprehensive papers, White *et al.* [41] and Chow *et al.* [42] systematically explored the effects of synaptic time constants on the firing period of individual neurons in inhibitory networks. In their analyses, the sensitivity of the firing period to the synaptic time constant is largely dependent on I and it is larger when the applied current is smaller, which is different from our finding that the macroscopic frequency is more sensitive to the time constants when I is large (figure 6*a,b,d,e*). Their result makes sense for individual neurons since at low drives, the neuron is close to the bifurcation from rest and, so, will be more sensitive to perturbations. Our situation is different since there are two ‘competing’ factors. To better understand why our results are different from the Chow *et al.* and White *et al.* work, the results of the adjoint method were compared for a higher current $I = 4$ and a lower one $I = 1.5$ with fixed parameters of $p_{\text{syn}} = 0.2$ and $\sigma = 2$. Figure 9*a* shows the PRFs ($h_{2(0)}^*$) and figure 9*b* shows the firing probability of the periodic orbit with $I = 4$ and $I = 1.5$. The macroscopic PRF is smaller with larger I , which would be related to the fact that the PRF of an individual neuron is smaller with larger I [43] (i.e. the individual neuron is farther to its bifurcation point). On the other hand, the large amplitude oscillation in firing probability is obtained with $I = 4$ (figure 9*b*), because it is far from the supercritical HB point. From equations (3.4) and (3.5), the sensitivity of frequency, $\partial\omega/\partial\tau_r$ and $\partial\omega/\partial\tau_d$, is obtained by averaging of the

time course of $h_{2(0)}^* \cdot R_r$ and $h_{2(0)}^* \cdot R_d$, respectively. Thus, we show these time courses in figure 9c,d. Regardless of smaller PRF of $I = 4$, they have larger negative values, which leads to high sensitivity. These larger values are caused because the large amplitude oscillation in firing probability influences these time courses through R_r in equation (3.3) and R_d in equation (3.6). Thus, the high sensitivity is obtained even though the macroscopic PRF is larger under the condition of smaller I (figure 9c,d). We can also see that this feature is apparent in the case of τ_r in figure 9c, which leads to large $\Delta\omega_r/\Delta\omega_d$.

From these sensitivity analyses, we see that the analyses of firing probability allow for a more quantitative evaluation of population activity, that would be difficult with only numerical computations of the finite-size neuron network [41,42]. The macroscopic PRF with its link to the microscopic one (equation (2.30)) enables us to understand the complicated relationships between microscopic structure and macroscopic oscillatory dynamics, and it cannot be achieved by the phase reduction of the simplified firing rate models of neuronal population [21,44].

Other relatively minor (hence small) types of interactions can also be taken into account as perturbations in this framework. In the electronic supplementary material, we evaluated the influence of a small number of gap junctions on the frequency of oscillation and obtained good agreement between theoretical prediction and numerical computations (see the electronic supplementary material, text S2 and figure S2 for details).

Shunting inhibition has been experimentally shown to promote macroscopic gamma oscillations [35]. Using weak coupling analysis and in the strongly oscillatory regime (all neurons fire on every cycle), the Gutkin group has shown that shunting inhibition can destabilize the perfectly synchronized state [11,30]. Our results show that the effects of shunting are complicated and depend on other parameters in the model. For example with lower bias currents, increasing the reversal potential of the GABA synapse destroys the gamma oscillation while at higher bias currents, there is only a small interval of reversal potentials where the gamma oscillations are destroyed. Thus, far from the bifurcation point (high drive), shunting inhibition can enhance gamma but near the bifurcation to gamma (low bias), the reduction in inhibitory drive (increased GABA reversal) pushes the population towards an asynchronous steady state. These non-trivial properties are observed not only by the modified theta model, but also by the conductance-based neuron model (see the electronic supplementary material, text S3 and figure S3 for details). Furthermore, it is also known that the reversal potential is higher than the resting membrane potential in the immature brain [45]; the systematic analyses of our model would be effective to understand the dynamics of the immature brain.

References

1. Wang XJ. 2010 Neurophysiological and computational principles of cortical rhythms in cognition. *Physiol. Rev.* **90**, 1195–1268. (doi:10.1152/physrev.00035.2008)
2. Yamaguchi S, Isejima H, Matsuo T, Okura R, Yagita K, Kobayashi M, Okamura H. 2003 Synchronization of cellular clocks in the suprachiasmatic nucleus. *Science* **302**, 1408–1412. (doi:10.1126/science.1089287)
3. Garcia-Ojalvo J, Elowitz MB, Strogatz SH. 2004 Modeling a synthetic multicellular clock: repressilators coupled by quorum sensing. *Proc. Natl Acad. Sci. USA* **101**, 10 955–10 960. (doi:10.1073/pnas.0307095101)
4. Horikawa K, Ishimatsu K, Yoshimoto E, Kondo S, Takeda H. 2006 Noise-resistant and synchronized oscillation of the segmentation clock. *Nature* **441**, 719–723. (doi:10.1038/nature04861)

In the sparse firing state, it is difficult to systematically explore parameter space because the simulations must necessarily be long and involve many cells (in contrast to systems where every neuron fires in each cycle). For this reason, population models are a very useful tool as they result in PDEs that are deterministic. The proposed model enables us to evaluate the effect of synaptic interactions more rigorously than the conventional theta model. We demonstrated that the precise evaluation of synaptic interactions is important because the time constants and reversal potential greatly altered macroscopic properties (stability, frequency and PRF) of gamma oscillations as they are varied even within biologically plausible ranges. Thus, the proposed model and methods could be a key technique for elucidation of the micro–macro relationship of the gamma oscillation and its functional roles. Although we restricted ourselves only to networks of inhibitory neurons so as to limit the number of parameters studied, the same methods could be used to analyse networks of excitatory and inhibitory neurons. Such extensions would be very useful in the study of phase-locking of gamma across different areas as we could then use the derived adjoint functions (PRFs) to couple macroscopic population rhythms. Furthermore, we believe that the adjoint method for simultaneous equations composed of ODEs for interactions and a PDE for the probability distribution, that we have developed in this study, will provide a useful starting point for an in-depth understanding of various collective oscillations in biology that are composed of individual noisy oscillators with complex interactions including circadian oscillation in suprachiasmatic nucleus [2], quorum-sensing bacteria [3] and somite segmentations in vertebrate embryos [4].

Funding statement. This study was supported by Grants-in-Aid for Scientific Research (23680024 to K.K. and 23240065 to Y.J.). K.K. was also supported by SCOPE (112103010). G.B.E. was supported by National Science Foundation grant no. DMS1219754.

Endnotes

¹The FPE is numerically integrated by the Crank–Nicolson method. In the case of solving the adjoint equation, the Lax–Wendroff scheme is further adopted in order to improve the precision of the numerical integration. We basically divide the phase $(-\pi, \pi]$ into 200 bins except for figure 3 and blue lines in figure 4a,b, in which 5000 bins are adopted for accurate computation. In figure 4a,b, the results of 200 and 5000 bins are in good agreement, indicating that 200 bins are enough to calculate macroscopic phase response functions. For the bifurcation analyses by XPPAUT, centred difference for 100 bins is adopted and numerically integrated by CVODE [31]. This scheme preserves the total probability. Because of this conservation, there is always a zero eigenvalue. To eliminate this eigenvalue and thus fix the mass, we reduce the dimension to 99 equations and set, say, $P_1 dx = 1 - dx \sum_{j=2}^N P_j$. Here, $dx = 2\pi/100$. With the elimination of the zero eigenvalue, we can use AUTO to compute steady states and their stability.

5. Wang XJ, Buzsáki G. 1996 Gamma oscillation by synaptic inhibition in a hippocampal interneuronal network model. *J. Neurosci.* **16**, 6402–6413.
6. Womelsdorf T, Schoffelen JM, Oostenveld R, Singer W, Desimone R, Engel AK, Fries P. 2007 Modulation of neuronal interactions through neuronal synchronization. *Science* **316**, 1609–1612. (doi:10.1126/science.1139597)
7. Rodríguez E, George N, Lachaux JP, Martinerie J, Renault B, Varela FJ. 1999 Perception's shadow: long-distance synchronization of human brain activity. *Nature* **397**, 430–433. (doi:10.1038/17120)
8. Bartos M, Vida I, Jonas P. 2007 Synaptic mechanisms of synchronized gamma oscillations in inhibitory interneuron networks. *Nat. Rev. Neurosci.* **8**, 45–56. (doi:10.1038/nrn2044)
9. Fisahn A, Contractor A, Traub RD, Buhl EH, Heinemann SF, McBain CJ. 2004 Distinct roles for the kainate receptor subunits GluR5 and GluR6 in kainate-induced hippocampal gamma oscillations. *J. Neurosci.* **24**, 9658–9668. (doi:10.1523/JNEUROSCI.2973-04.2004)
10. Whittington MA, Traub RD, Jefferys JG. 1995 Synchronized oscillations in interneuron networks driven by metabotropic glutamate receptor activation. *Nature* **373**, 612–615. (doi:10.1038/373612a0)
11. Stiefel KM, Wespapat V, Gutkin B, Tegnér F, Singer W. 2005 Phase dependent sign changes of GABAergic synaptic input explored in-silico and in-vitro. *J. Comput. Neurosci.* **19**, 71–85. (doi:10.1007/s10827-005-0188-3)
12. Cardin JA, Carlén M, Meletis K, Knoblich U, Zhang F, Deisseroth K, Tsai L, Moore CI. 2009 Driving fast-spiking cells induces gamma rhythm and controls sensory responses. *Nature* **459**, 663–667. (doi:10.1038/nature08002)
13. Buzsáki G, Horvath Z, Urioste R, Hetke J, Wise K. 1992 High-frequency network oscillation in the hippocampus. *Science* **256**, 1025–1027. (doi:10.1126/science.1589772)
14. Fisahn A, Pike FG, Buhl EH, Paulsen O. 1998 Cholinergic induction of network oscillations at 40 Hz in the hippocampus in vitro. *Nature* **394**, 186–189. (doi:10.1038/28179)
15. Ermentrout B. 1996 Type I membranes, phase resetting curves, and synchrony. *Neural Comput.* **8**, 979–1001. (doi:10.1162/neco.1996.8.5.979)
16. Kuramoto Y. 1984 *Chemical oscillations, waves, and turbulence*. New York, NY: Springer.
17. Pikovsky A, Rosenblum M, Kurths J. 2001 *Synchronization: a universal concept in nonlinear science*. Cambridge, UK: Cambridge University Press.
18. Kanamaru T, Sekine M. 2005 Synchronized firings in the networks of class 1 excitable neurons with excitatory and inhibitory connections and their dependences on the forms of interactions. *Neural Comput.* **17**, 1315–1338. (doi:10.1162/0899766053630387)
19. Kawamura Y, Nakao H, Arai K, Kori H, Kuramoto Y. 2008 Collective phase sensitivity. *Phys. Rev. Lett.* **101**, 024101. (doi:10.1103/PhysRevLett.101.024101)
20. Kawamura Y, Nakao H, Kuramoto Y. 2011 Collective phase description of globally coupled excitable elements. *Phys. Rev. E* **84**, 046211. (doi:10.1103/PhysRevE.84.046211)
21. Akam T, Oren I, Mantoan L, Ferenczi E, Kullmann DM. 2012 Oscillatory dynamics in the hippocampus support dentate gyrus-CA3 coupling. *Nat. Neurosci.* **15**, 763–768. (doi:10.1038/nn.3081)
22. Fourcaud-Trocmé N, Hansel D, Van Vreeswijk C, Brunel N. 2003 How spike generation mechanisms determine the neuronal response to fluctuating inputs. *J. Neurosci.* **23**, 11 628–11 640.
23. Pfeuty B, Mato G, Golomb D, Hansel D. 2003 Electrical synapses and synchrony: the role of intrinsic currents. *J. Neurosci.* **23**, 6280–6294.
24. Dipoppa M, Gutkin BS. 2013 Flexible frequency control of cortical oscillations enables computations required for working memory. *Proc. Natl Acad. Sci. USA* **110**, 12 828–12 833. (doi:10.1073/pnas.1303270110)
25. Brunel N, Wang XJ. 2003 What determines the frequency of fast network oscillations with irregular neural discharges? I. Synaptic dynamics and excitation-inhibition balance. *J. Neurophysiol.* **90**, 415–430. (doi:10.1152/jn.01095.2002)
26. Bartos M, Vida I, Frotscher M, Geiger JRP, Jonas P. 2001 Rapid signaling at inhibitory synapses in a dentate gyrus interneuron network. *J. Neurosci.* **21**, 2687–2698.
27. Gupta A, Wang Y, Markram H. 2000 Organizing principles for a diversity of GABAergic interneurons and synapses in the neocortex. *Science* **287**, 273–278. (doi:10.1126/science.287.5451.273)
28. McCormick DA, Huguenard JR. 1992 A model of the electrophysiological properties of thalamocortical relay neurons. *J. Neurophysiol.* **68**, 1384–1400.
29. Ermentrout B, Pascal M, Gutkin B. 2001 The effects of spike frequency adaptation and negative feedback on the synchronization of neural oscillators. *Neural Comput.* **13**, 1285–1310. (doi:10.1162/08997660152002861)
30. Jeong HY, Gutkin B. 2005 Study on the role of GABAergic synapses in synchronization. *Neurocomputing* **65**, 859–868. (doi:10.1016/j.neucom.2004.10.063)
31. Ly C, Ermentrout GB. 2010 Analysis of recurrent networks of pulse-coupled noisy neural oscillators. *SIAM J. Appl. Dyn. Syst.* **9**, 113–137. (doi:10.1137/090756065)
32. Risken H. 1985 *The Fokker–Planck equation: methods of solution and applications*. Berlin, Germany: Springer.
33. Gerstner W, Kistler WM. 2002 *Spiking neuron models: single neurons, populations, plasticity*. Cambridge, UK: Cambridge University Press.
34. Ermentrout B. 2002 *Simulating, analyzing, and animating dynamical systems: a guide to XPPAUT for researchers and students*, vol. 14. Philadelphia, PA: Society for Industrial and Applied Mathematics.
35. Vida I, Bartos M, Jonas P. 2006 Shunting inhibition improves robustness of gamma oscillations in hippocampal interneuron networks by homogenizing firing rates. *Neuron* **49**, 107–118. (doi:10.1016/j.neuron.2005.11.036)
36. Sohal VS, Zhang F, Yizhar O, Deisseroth K. 2009 Parvalbumin neurons and gamma rhythms enhance cortical circuit performance. *Nature* **459**, 698–702. (doi:10.1038/nature07991)
37. Brunel N, Hansel D. 2006 How noise affects the synchronization properties of recurrent networks of inhibitory neurons. *Neural Comput.* **18**, 1066–1110. (doi:10.1162/neco.2006.18.5.1066)
38. Bartos M, Vida I, Frotscher M, Meyer A, Monyer H, Geiger JRP, Jonas P. 2002 Fast synaptic inhibition promotes synchronized gamma oscillations in hippocampal interneuron networks. *Proc. Natl Acad. Sci. USA* **99**, 13 222–13 227. (doi:10.1073/pnas.192233099)
39. Kilpatrick ZP, Ermentrout B. 2011 Sparse gamma rhythms arising through clustering in adapting neuronal networks. *PLoS Comput. Biol.* **7**, e1002281. (doi:10.1371/journal.pcbi.1002281)
40. Maex R, De Schutter E. 2003 Resonant synchronization in heterogeneous networks of inhibitory neurons. *J. Neurosci.* **23**, 10 503–10 514.
41. White JA, Chow CC, Ritt J, Soto-Treviño C, Kopell N. 1998 Synchronization and oscillatory dynamics in heterogeneous, mutually inhibited neurons. *J. Comput. Neurosci.* **5**, 5–16. (doi:10.1023/A:1008841325921)
42. Chow CC, White JA, Ritt J, Kopell N. 1998 Frequency control in synchronized networks of inhibitory neurons. *J. Comput. Neurosci.* **5**, 407–420. (doi:10.1023/A:1008889328787)
43. Brown E, Moehlis J, Holmes P. 2004 On the phase reduction and response dynamics of neural oscillator populations. *Neural Comput.* **16**, 673–715. (doi:10.1162/089976604322860668)
44. Battaglia D, Brunel N, Hansel D. 2007 Temporal decorrelation of collective oscillations in neural networks with local inhibition and long-range excitation. *Phys. Rev. Lett.* **99**, 238106. (doi:10.1103/PhysRevLett.99.238106)
45. Ben-Ari Y. 2002 Excitatory actions of GABA during development: the nature of the nurture. *Nat. Rev. Neurosci.* **3**, 728–739. (doi:10.1038/nrn920)